

Preliminary report on obsidian petrography from the Transcarpathian region in Ukraine

Yoshimitsu Suda^{1*}, Masayoshi Yamada²,
Sergii Ryzhov³ and Vadim Stepanchuk⁴

Abstract

This paper reports the field occurrence, mineralogy, and whole-rock chemistry of the obsidian from the Neogen Carpathian volcanic arc area. The study area encompasses the Transcarpathian (Zakarpattia) region in Ukraine. A mafic xenolith comprising of a plagioclase, amphibole, and olivine mineral assemblage was found from the obsidian in this area. SEM-EDS analysis indicates that the olivine has high magnesium content. The forsterite (Mg_2SiO_4) content varies from 77% to 80%. The chemical composition of plagioclase remains constant, and is enriched in calcium. The anorthite ($CaAl_2Si_2O_8$) content varies from 89% to 94%. The amphibole is classified into the tschermakite following the nomenclature of Leake et al. (1997). Based on the compositions of the amphibole and the plagioclase, pressure and temperature conditions of the mafic xenolith were estimated to be 4.5–7.9 kbar and 1185–1358°C respectively. These results indicate that this mineral aggregate is not genetically associated with the rhyolitic magma from which the obsidian was derived, but is considered to be of an exotic xenolith originated from the gabbroic rocks of the lower crustal level of the Carpathian volcanic arc. The finding of mafic xenolith will help in characterizing the obsidian from this area, and is a key in understanding the tectonic and evolutionary history of the Carpathian volcanic arc.

Keywords: obsidian; Transcarpathian; Ukraine; geology; petrography; geochemistry

1. Introduction

The Carpathian mountain range in Ukraine is located in the northeastern part of the Alpine orogenic belt (Rosenbaum and Lister 2002; Schmid et al. 2004, 2008) (Figure 1a). The subduction of the European Plate beneath the Pannonian Plate formed the Carpathian arc and Pannonian Basin during the Mesozoic era (Mason et al. 1998; Seghedi et al. 2004; Pecskey et al. 2006, 2009; Rasser and Harzhauser 2008). The Carpathian mountain range is generally composed of molasses and flysch belts. The components are the equivalents of an accretionary complex that formed by the subduction of the European Plate (Foldvary 1988).

The Carpathian volcanic arc is situated between the

Pannonian Basin and the Carpathian mountain range, and it is characterized by the occurrence of the Neogene calc-alkaline volcanic rocks with andesitic to rhyolitic composition (Pecskey et al. 2009; Lexa 2010). The Pannonian basin is the back-arc basin that formed by the upwelling of the upper mantle due to the subduction of the European Plate (Konecny et al. 2002). Most of this basin region is covered by volcanoclastic deposits and sediments (Foldvary 1988; Oszczypko 2004).

Pecskey et al. (2000) indicated that the Carpathian volcanic arc in the Transcarpathian (Zakarpattia Oblast) region is divided into the three areas: 1) outer arc volcanic area, 2) inner arc volcanic area, and 3) intermediate area (Figure 1b). The outer arc volcanic area is composed of a chain of volcanic mountains. The whole-rock K-Ar age of 13.4–9.1 Ma is reported from this area (Pecskey et al., 2000).

1 Center for Obsidian and Lithic Studies, Meiji University, 3670–8 Daimon, Nagawa-machi, Nagano 386–0601, Japan

2 Sarugakucho Branch, Center for Obsidian and Lithic Studies, Meiji University, 1–1 Kanda Surugadai, Tokyo 101–0064, Japan

3 Taras Shevchenko National University of Kiev, Department of Archaeology and Museum Studies, Volodymirska St. 64. Kyiv 01601, Ukraine

4 Institute of Archaeology, National Ukrainian Academy of Sciences, Geroiv Stalingrada ave., 04210, Kyiv-210, Ukraine

* Corresponding author: Y. Suda (geosuda@gmail.com)

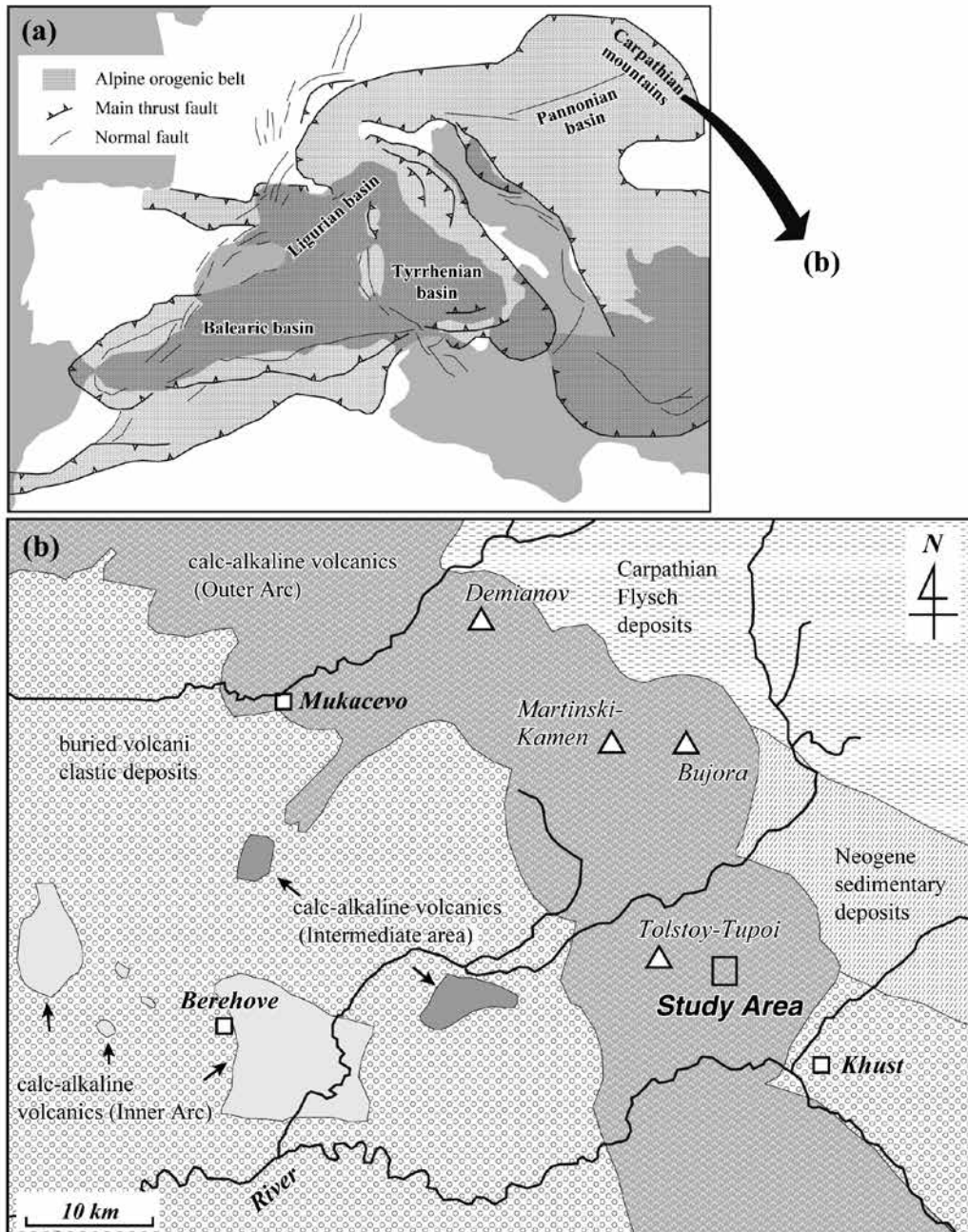


Figure 1 (a) Map of Alpine orogenic belt in Europe. Modified after Rosenbaum and Lister (2002).
 (b) Geological map of Transcarpathian region in the study area (Pecskay et al. 2000).

In August 2013, we performed a geological and archaeological field survey targeting the obsidian sources at the Tolstoy-Tupoi volcanic mountain (Pecskay et al. 2000). This mountain is a part of the outer arc volcanic area, and is located in the northwestern part of the Khust City (Figure 1b). Whole-rock K-Ar age of $10.6 \pm 0.5\text{Ma}$ (Pecskay et al., 2000) is determined from the pyroxene dacite in this volcanic mountain.

Previous studies have revealed that a cluster of obsidian sources can be found in this mountain area (e.g. Rosania et al. 2008). The obsidian in this area has been widely used as the lithic raw material for the production of obsidian

artefacts in the Central Europe and Mediterranean region (e.g. Yamada 2012, 2013). Furthermore, Lower, Middle and Upper Paleolithic occupations at the archaeological sites Malyj Rakovets IV and Rokosovo V seem to be closely associated with this cluster of obsidian sources (e.g. Gladilin and Sitlivyj 1990; Sitlivyi and Ryzhov 1992; Ryzhov et al. 2005, 2009; Stepanchuk et al. 2010; Ryzhov 2012).

Therefore, the geological characterization of the obsidian source in this mountain is significant for the provenance identification of the lithic raw material used in the manufacture of obsidian artefacts found in European archeological sites. This paper reports the preliminary results of field survey, and

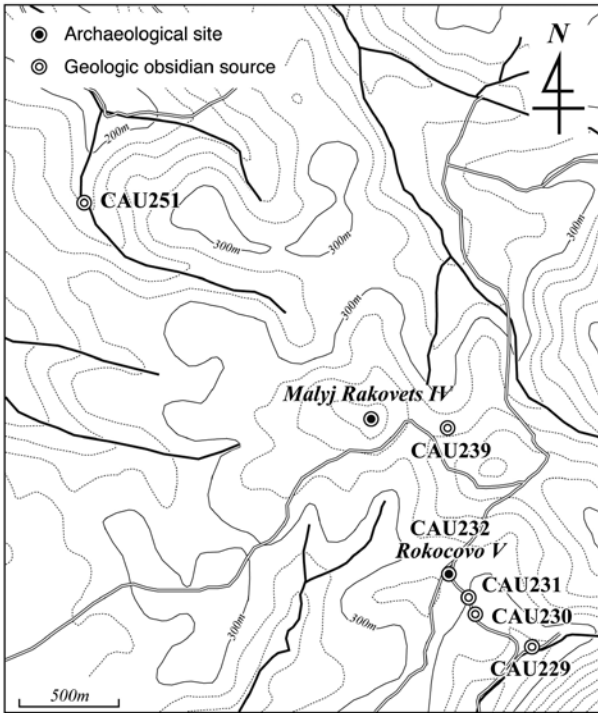


Figure 2 Topographic map showing the exact locations where the specimens were collected.

petrological analysis for the Carpathian obsidian in this area. Obsidian is defined as “a black or dark-colored volcanic glass, usually of rhyolitic composition, characterized by conchoidal fracture” after the definition by Jackson ed. (1997: p.441).

2. Specimens

2-1 Field occurrences

We collected obsidian samples from six sources in the study area (Figure 2: CAU229, 230, 231, 232, 239 and 251). Obsidian in the study area occurs naturally in the form of nodules within clayey loess (Figure 3). Their specific locations (i.e. longitude and latitude) are listed in Table 1.

Table 1. Locations and mineral assemblages of samples

Name	latitude (N)	longitude (E)	<i>phenocryst</i>						
			<i>glomeroporphyritic</i>			<i>isolated</i>			
			<i>ol-ag</i>	<i>opx-ag</i>	<i>pl-ag</i>	<i>pl</i>	<i>opx</i>	<i>ilm</i>	<i>hbl</i>
CAU229	48.22826 °	23.19027 °	×	○	○	○	○	○	○
CAU230	48.22967 °	23.18628 °	○	○	○	○	○	○	×
CAU231	48.23048 °	23.18591 °	×	○	○	○	○	○	×
CAU232	48.23162 °	23.18454 °	×	○	○	○	○	○	×
CAU239	48.23829 °	23.18453 °	○	○	○	○	○	○	×
CAU251	48.24856 °	23.15961 °	×	○	○	○	○	○	×

Abbreviations: *hbl*, hornblende; *ilm*, ilmenite; *pl*, plagioclase; *opx*, orthopyroxene; *ol*, olivine; *pl-ag*, pl aggregate; *opx-ag*, opx-pl-ilmenite aggregate; *ol-ag*, ol-pl-hbl aggregate.



Figure 3 In situ specimen from the CAU239 site in the study area.

All of the specimens collected are rounded in shape and their size varies from a few centimeters to several tens of centimeters. The specimens of larger size are found around a mountain ridge (the site of CAU239). The smaller nodules are mostly found around a valley (the sites of CAU229, 230 and 251).

2-2 Appearance and texture

The specimens collected are shown in Figure 4. Their surface is somewhat white due to hydration. The banded texture becomes even more distinct by the uneven weathering. Underneath their weathered surface the samples are completely lustrous or glassy with the characteristic black color.

Thin sections of all samples were prepared and observed under a petrologic microscope (Figure 5). The texture of all specimens is characterized by the foliation or the banded texture, in which minute phenocrysts (measuring some millimeters) are observed.

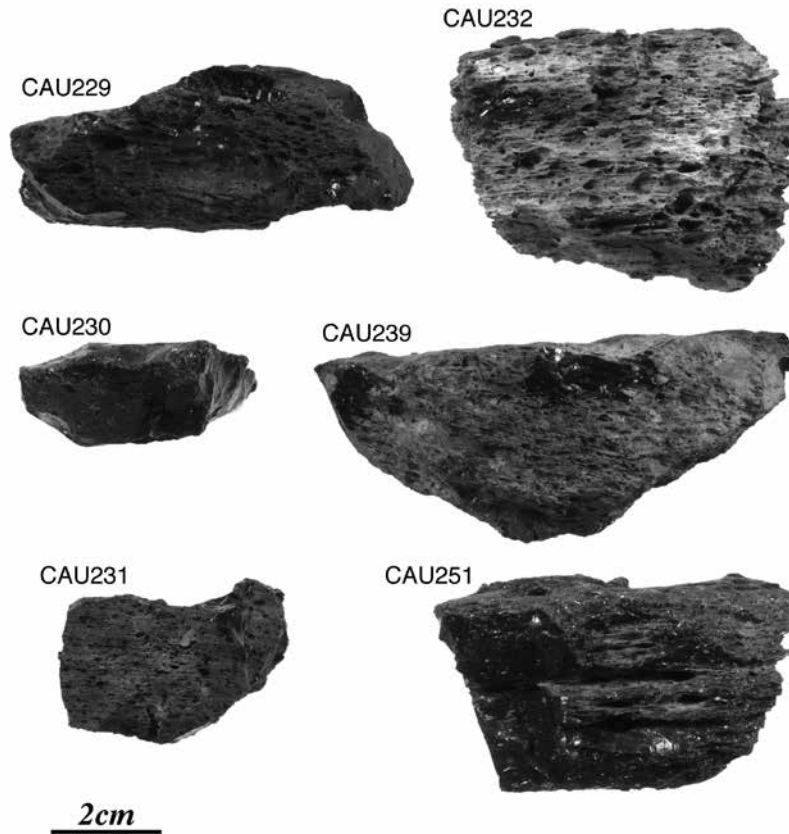


Figure 4 The specimens used in the present study.

3. Mineralogy

3-1 General components

The obsidian samples are composed of the matrix glass, crystallite (microphenocryst), and phenocryst. The major components for each of the specimens can be found in Table 1. Modal composition of the matrix glass is 95–96%, that of crystallite is 3–4%, and that of phenocryst reaches 1.1–1.6% for all of the specimens.

3-2 Matrix glass

The matrix glass is the most abundant component in the specimens. When observed under a polarized microscope, it is possible to see that the glassy matrix is characterized by colorless with high transparency under plane-polarized light conditions, and dark non-transparent under crossed polars. These results indicate the characteristics of the optically isotropic body.

3-3 Microphenocrysts

According to the glossary of geology (Jackson ed. 1997: p.155), crystallite is “a broad term applied to a minute body of unknown mineralogical composition or crystal form that does

not polarize light. Crystallites represent the initial stage of crystallization of a magma and of a glass”. On the other hand, the microlite is defined as a “microscopic crystal that polarizes light and has some determinable optical properties” (Jackson ed. 1997: p.407).

These definitions indicate that the microlite is relatively larger in size than the crystallite, and the microlite can be identified as a mineral with the help of polarized microscopy. The microphenocrysts that occur in the specimens cannot assign them as any type of a mineral under the polarized microscopy. Therefore, the microphenocrysts found in the specimens are all classified as “crystallites” following the definitions of the abovementioned glossary (Jackson ed. 1997). The occurrence of crystallite in the specimens takes the form of fine needles of a few microns in length. The foliated or banded texture developing in the specimens is characterized by the alignment and aggregate of these crystallites.

3-4 Phenocrysts

3-4-1 Occurrence

The occurrence of phenocrysts in the specimens is roughly classified into 1) isolated crystal, and 2) glomeroporphyritic

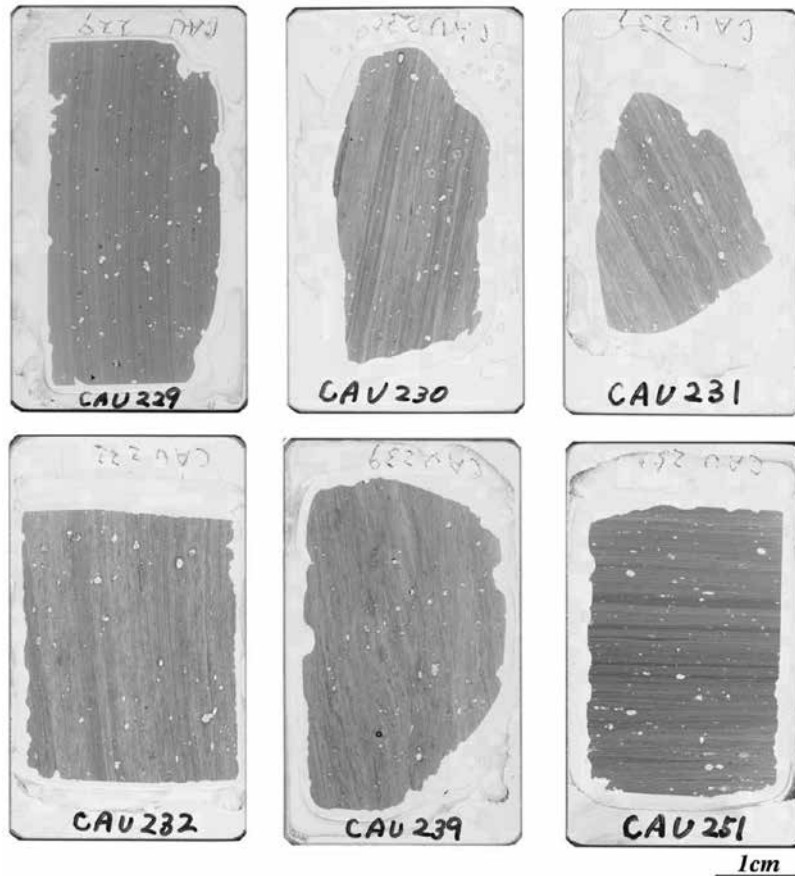


Figure 5 Thin sections of the specimens used in the present study.

aggregates (i.e. clot of crystals). Both types are found in all specimens. The mineral components of the phenocrysts are shown in Table 1.

3-4-2 Isolated crystal

The phenocryst formed by an isolated crystal includes plagioclase, orthopyroxene, amphibole and opaque minerals. The plagioclase phenocryst is found in all specimens, and it has a characteristic euhedral shape with a length of 0.5–2.0 mm. The orthopyroxene phenocrysts are also found in all specimens and have a euhedral shape with 0.5–1.0 mm in length, and it sometimes coexists with fine grains of ilmenite. Euhedral amphibole is found in the CAU229 specimen. The grain size is 10–100 μm in length. The opaque mineral is composed of ilmenite and pyrite. Their grain sizes are several tens of microns. Ilmenite can be found in all specimens, while pyrite is found predominantly in the CAU229 specimen.

3-4-3 Glomeroporphyritic aggregate

The glomeroporphyritic aggregate is divided into three types on the basis of their mineralogical composition: 1) olivine + plagioclase + amphibole (Figure 6a: ol-bearing aggregate), 2) orthopyroxene + plagioclase + ilmenite

(Figure 6b: opx-bearing aggregate), and 3) multiple grains of plagioclase (i.e. plagioclase aggregate).

The olivine-bearing aggregate occurs in the CAU230, 232, 239 and 251 specimens (Table 1). This aggregate is <2.0 mm in diameter, and composed of euhedral and subdural olivine, plagioclase and amphibole grains. The modal composition of the olivine in this aggregate reaches up to 40%; whereas amphibole and plagioclase are ca. 30%. These occurrences indicate that this aggregate corresponds to mafic rocks with ultramafic composition ($\text{SiO}_2 < 45\text{wt.}\%$). According to the classification of the gabbroic rocks (Streckeisen 1976), this aggregate is classified into the amphibole-bearing troctolite.

The opx-bearing aggregate occurs in all specimens (Table 1). This aggregate is <2.0 mm in diameter, and it is composed of euhedral to subdural grains of plagioclase and orthopyroxene. The mineralogical composition of this aggregate relates to a norite according to the classification of the gabbroic rocks (Streckeisen 1976).

The plagioclase aggregate is also found in all specimens. The aggregate is 0.1–0.3 mm in diameter, and it is composed of the aggregate of several euhedral plagioclase grains with of 10–100 μm in length.

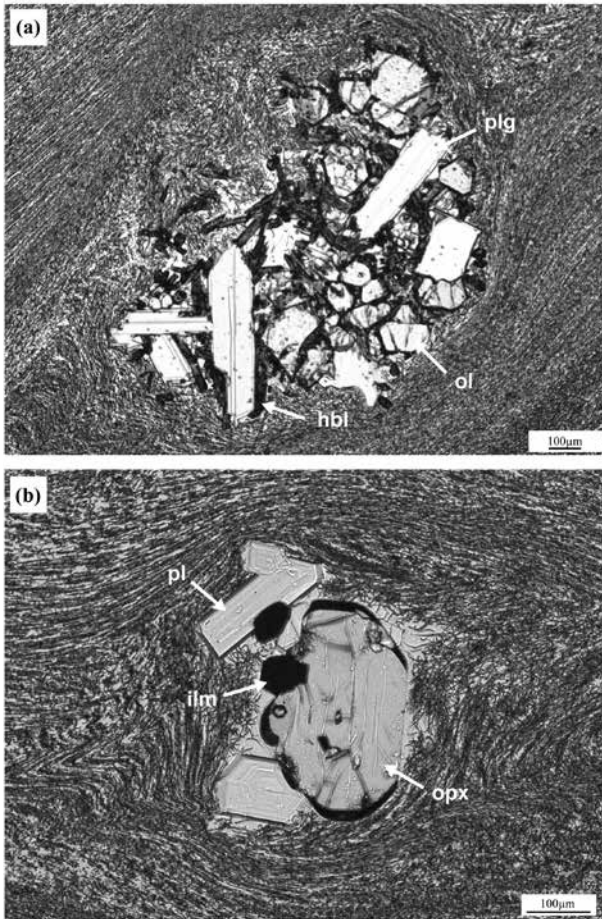


Figure 6 Photomicrographs of the phenocryst of plagioclase (pl) + olivine (ol) + hornblende (hbl) aggregate in the CAU230 specimen (a), and that of plagioclase (pl) + ilmenite (ilm) + orthopyroxene (opx) aggregate in the CAU229 specimen (b).

4. Mineral chemistry

4-1 Analytical method

SEM-EDS (Scanning Electron Microscopy Energy Dispersive Spectroscopy) analysis was performed to determine the elemental composition of the minerals in the specimens. The analysis was carried out with the non-standard method using the software of the JED Series Analysis Station. Accuracy and reliability of the results generated with this method are approximately estimated by the comparison with the results of analysis by the EPMA (Electron Probe Micro Analyzer) method (Appendix 1). The representative composition of plagioclase, clinopyroxene, olivine, amphibole and ilmenite in the specimens are shown in Tables 2–4.

SEM-EDS analysis was carried out using a JEOL JSX-3100II housed at the Center for Obsidian and Lithic Studies (COLS), Meiji University. EPMA analysis was carried out using a JEOL JXA-8200 at the National Institute of Polar

Research (NIPR), Japan.

4-2 Crystallite

The crystallites are distinguished in the backscattered electron (BSE) image by its brightness, while the matrix glass is darker, because of the chemical contrast between these portions (Figure 9c). The crystallites are relatively rich in heavy elements with respect to the matrix glass (Figures 9d-f). From this BSE image, the modal composition of crystallite in the specimens was estimated to be ca. 3.0%.

The result of element mapping further indicated that calcium, iron and magnesium are enriched in crystallites with respect to the matrix glass. The results of element mapping suggest that the crystallite analyzed in the present study would be the equivalent of the Ca-pyroxene or clinopyroxene crystallite.

4-3 Plagioclase

4-3-1 Occurrence

The BSE images of the plagioclase in the specimens indicate two types: 1) the plagioclase with zonal structure, and 2) the plagioclase without zonal structure (i.e. compositionally uniform). Both types are found in all specimens. The zonal structure type can also be identified by means of a polarization microscope.

4-3-2 Plagioclase with zonal structure

The plagioclase with zonal structure occurs as isolated phenocrysts, within opx-bearing aggregates, and plagioclase aggregates. The zonal structure type is completely absent in the ol-bearing aggregate.

Results of BSE imagery indicate that some plagioclase with zonal structure have distinct core, mantle and rim portions. The core is several microns in size and it is characterized by its irregular shape, or edges with inhomogeneous compositional texture. The mantle completely surrounds the core, which is also of irregular shapes or with inhomogeneous compositional texture at its edges. On the other hand, the rim is characterized by the distinct texture of oscillatory zonal structure. Occurrences of these kinds of structures suggest that the core and mantle portions experience the dissolution and chemical diffusion processes, while the rim portion experiences the normal crystal growth from molten magma or melt (e.g. Shcherbakov et al. 2011).

The results of elemental mapping can be found in Figure 7. The results indicate that the concentration of sodium (Na) is clearly decreasing from the core to the rim. On the other hand, the concentration of calcium is increasing from the core to the rim. The elemental analysis by means of SEM-EDS indicates that the anorthite (An: $\text{CaAl}_2\text{Si}_2\text{O}_8$) and albite (Ab: $\text{NaAlSi}_3\text{O}_8$) content of plagioclase is varied from $\text{An}_{60}\text{Ab}_{40}$ to

An₈₈Ab₁₂ in the core–mantle portions, and from An₄₉Ab₅₁ to An₆₂Ab₃₈ in the rim portions (Figure 8; Table 2).

4-3-3 Plagioclase without zonal structure

The plagioclase without zonal structure occurs as isolated phenocrysts, and within ol-bearing aggregate. This type of plagioclase is completely absent in opx-bearing aggregate and the plagioclase aggregate.

Their BSE images indicate that this type of plagioclase does not show any compositional inhomogeneity, as it is completely uniform. Results of the SEM-EDS elemental analysis indicate that the composition the plagioclase grains are varied from An₈₉Ab₁₁ to An₉₄Ab₆ (Figure 8; Table 2). This means that the compositions of the plagioclase without zonal structure do not overlap with those of the plagioclase with the zonal structure. Namely, the plagioclases with diverse origins coexisted within a single specimen.

4-4 Orthopyroxene

Orthopyroxene occurs as isolated phenocryst, and in opx-bearing aggregate. BSE images indicate that some orthopyroxene occur as isolated phenocryst have zonal structure (Figure 9a). The core portion is relatively bright in comparison to the rim portion. The results of SEM-EDS elemental mapping support this conclusion as well, because the concentration of magnesium is increasing slightly from core to rim (Figure 9b).

Compositions of orthopyroxene are shown in the wollastonite (Wo: Ca₂Si₂O₆)-enstatite (En: Mg₂Si₂O₆)-ferrosilite (Fs: Fe₂Si₂O₆) ternary diagram (Figure 10a). The compositions do not have a wide range. The compositions are varied from Wo₄₂Fs₅₅En₃ to Wo₄₉Fs₄₉En₂ (Table 3), which is classified into the ferrosilite (Figure 10a). The orthopyroxene with compositional zoning texture cannot be detected with the

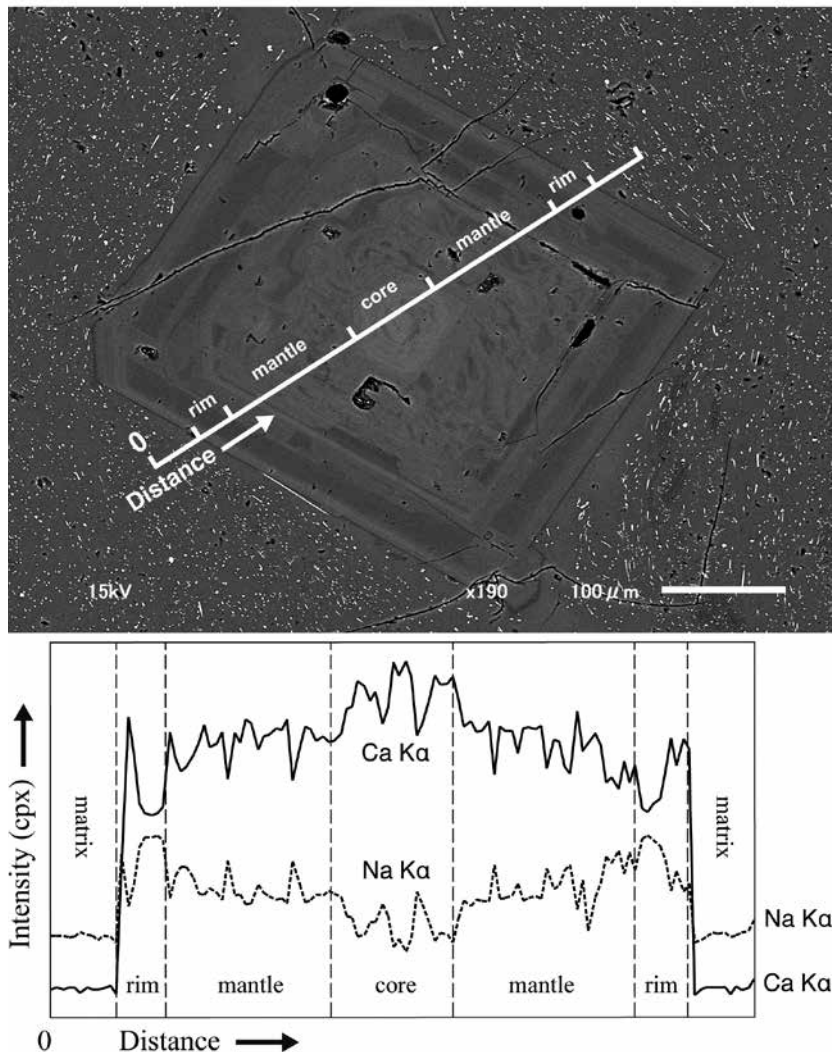


Figure 7 Backscattered electron (BSE) image and result of line analysis by SEM-EDS for the plagioclase with typical texture of oscillatory bands from the CAU239 specimen.

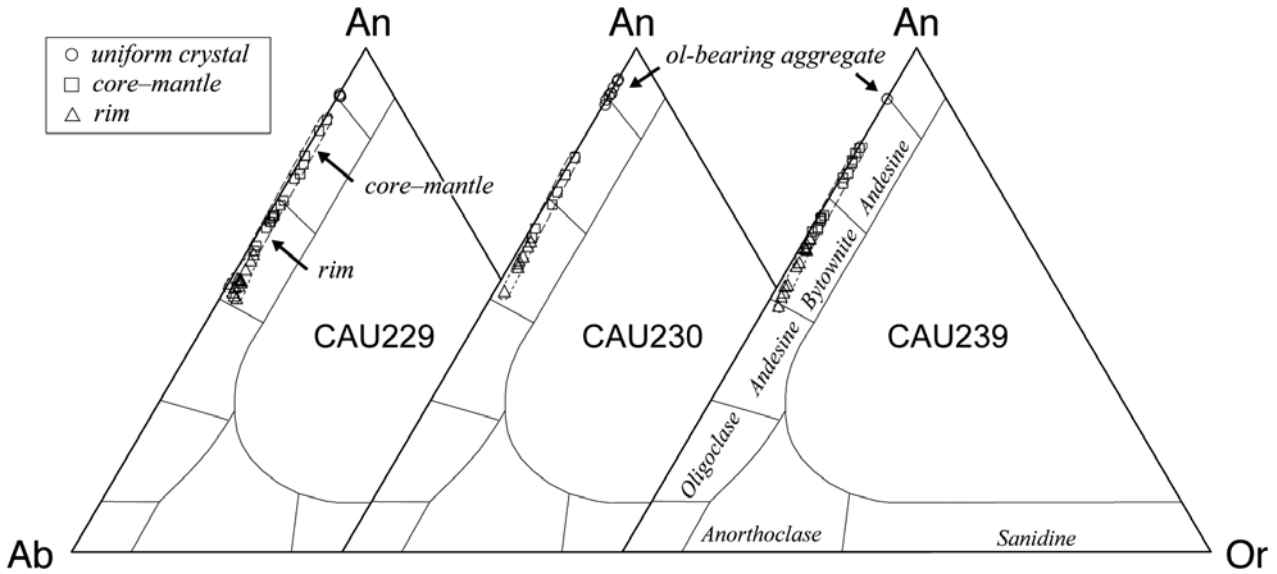


Figure 8 An ($\text{CaAl}_2\text{Si}_2\text{O}_8$)-Ab ($\text{NaAlSi}_3\text{O}_8$)-Or (KAlSi_3O_8) ternary diagrams indicating the compositional variation of the plagioclase in the CAU229, CAU230 and CAU239 specimens.

Table 2. Representative compositions of plagioclase by SEM-EDS analysis

sample	CAU229					CAU230					CAU239				
	isolated	isolated	isolated	pl-ag	opx-ag	ol-ag	isolated	isolated	isolated	opx-ag	ol-ag	isolated	opx-ag	opx-ag	opx-ag
point	uni	core	mantle	rim	rim	uni	core	mantle	rim	rim	uni	core	mantle	rim	rim
SiO ₂	45.24	53.53	47.12	55.47	54.14	44.81	49.60	52.94	52.95	54.73	45.46	48.41	53.23	56.32	53.14
TiO ₂	0.00	0.11	0.08	0.00	0.00	0.15	0.14	0.00	0.00	0.14	0.00	0.10	0.08	0.10	0.00
Al ₂ O ₃	35.01	29.79	34.07	28.43	29.73	35.31	32.26	30.28	30.16	28.57	34.48	33.20	29.75	27.83	30.08
FeO	0.51	0.00	0.23	0.13	0.13	0.63	0.29	0.15	0.31	0.33	0.73	0.19	0.42	0.24	0.17
MnO	0.03	0.04	0.02	0.06	0.00	0.00	0.00	0.00	0.00	0.09	0.00	0.06	0.00	0.00	0.00
MgO	0.00	0.00	0.00	0.00	0.00	0.00	0.00	0.00	0.00	0.00	0.02	0.00	0.00	0.00	0.00
CaO	18.20	12.01	16.67	10.22	11.55	18.43	14.90	12.39	12.15	10.55	18.15	15.75	12.06	9.74	12.41
Na ₂ O	1.00	4.33	1.78	5.22	4.25	0.67	2.72	4.03	4.22	5.26	1.11	2.27	4.26	5.39	4.05
K ₂ O	0.01	0.19	0.03	0.47	0.20	0.00	0.09	0.20	0.21	0.31	0.04	0.04	0.20	0.38	0.15
total	100.00	100.00	100.00	100.00	100.00	100.00	100.00	99.99	100.00	99.98	99.99	100.02	100.00	100.00	100.00
O =	8	8	8	8	8	8	8	8	8	8	8	8	8	8	8
Si	2.089	2.418	2.161	2.498	2.439	2.070	2.263	2.395	2.397	2.472	2.101	2.213	2.410	2.530	2.403
Ti	0.000	0.004	0.003	0.000	0.000	0.005	0.005	0.000	0.000	0.005	0.000	0.003	0.003	0.003	0.000
Al	1.905	1.586	1.842	1.509	1.579	1.922	1.735	1.614	1.609	1.521	1.878	1.789	1.587	1.473	1.603
Fe ²⁺	0.018	0.000	0.008	0.004	0.004	0.022	0.010	0.005	0.011	0.011	0.025	0.007	0.014	0.008	0.006
Mn	0.001	0.002	0.001	0.002	0.000	0.000	0.000	0.000	0.000	0.003	0.000	0.002	0.000	0.000	0.000
Mg	0.000	0.000	0.000	0.000	0.000	0.000	0.000	0.000	0.000	0.000	0.001	0.000	0.000	0.000	0.000
Ca	0.900	0.581	0.819	0.493	0.558	0.912	0.728	0.601	0.589	0.511	0.899	0.772	0.585	0.469	0.601
Na	0.090	0.379	0.158	0.456	0.371	0.060	0.241	0.353	0.370	0.461	0.099	0.201	0.374	0.469	0.355
K	0.001	0.011	0.002	0.027	0.011	0.000	0.005	0.012	0.012	0.018	0.002	0.002	0.012	0.022	0.009
An%	90.9	59.9	83.7	50.5	59.3	93.8	74.8	62.2	60.6	51.6	89.8	79.1	60.3	48.8	62.3

SEM-EDS method of analysis. The reason for this may be the limited resolution of the EDS method.

4-5 Olivine

Olivine predominantly occurs in the ol-bearing aggregate. Compositions of the olivine are shown in the tephroite (Te: MnSiO_4)-forsterite (Fo: Mg_2SiO_4)-fayalite (Fa: Fe_2SiO_4) ternary diagram (Figure 10b). The compositions of the olivine in all specimens are varied from $\text{Te}_0\text{Fo}_{77}\text{Fa}_{23}$ to $\text{Te}_0\text{Fo}_{80}\text{Fa}_{20}$ (Table 3). These are characteristically rich in magnesium contents.

4-6 Amphibole

The structural formulae of amphibole are calculated based on O=23 per unit cell, and the $\text{Fe}^{2+}/\text{Fe}^{3+}$ ratio was estimated on the basis of total cations excluding Ca, Na and K (Leake et al. 1997). The results of this calculation can be found in Table 4. Amphibole occurs in the phenocryst of ol-bearing aggregate that was analyzed.

The results indicate that the Si [tetrahedral site] content varied from 6.04 to 6.21, while the Na + K [A site] content varied from 0.27 to 0.44 (Table 4). According to the

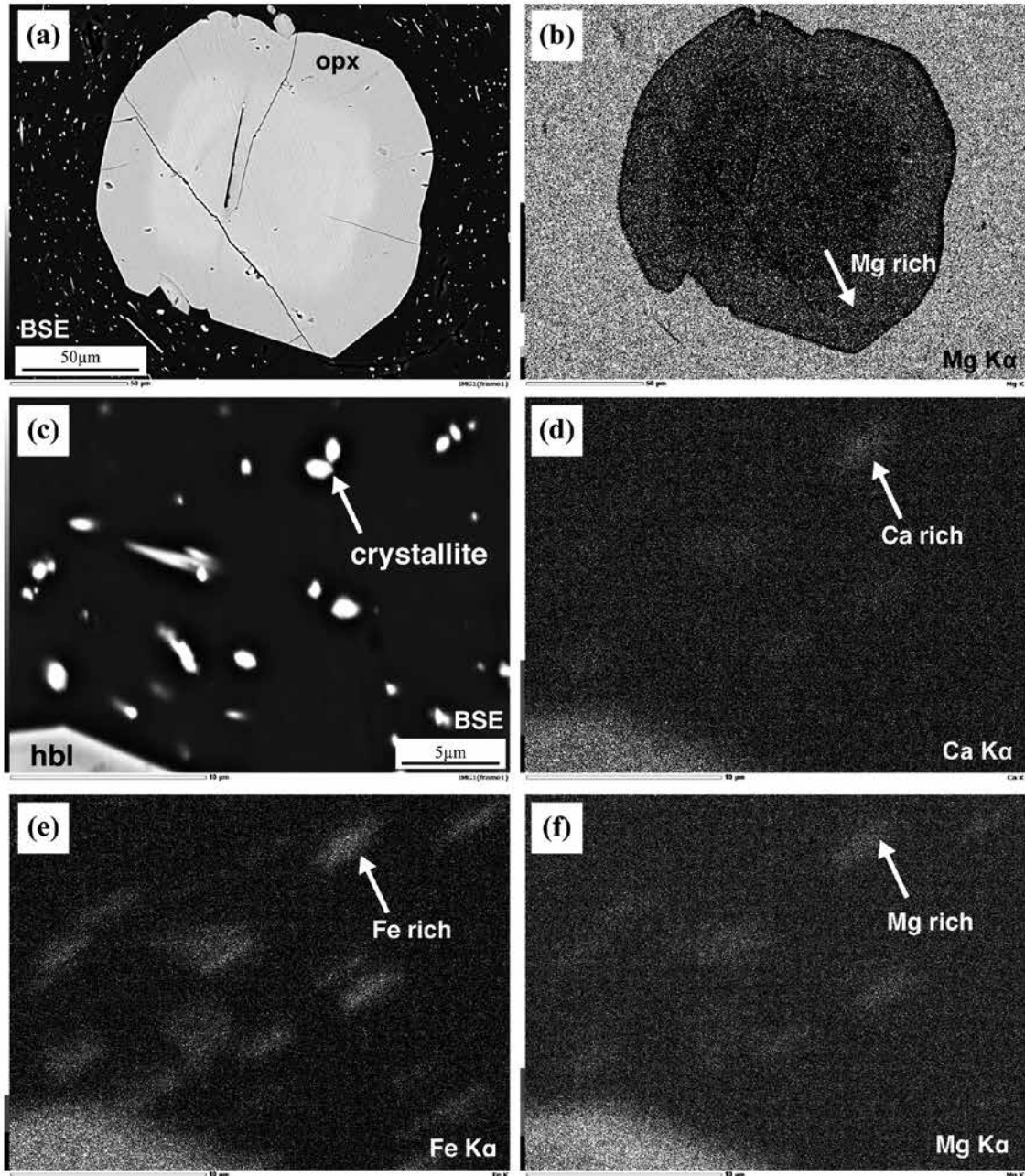


Figure 9 (a) Backscattered electron (BSE) image of the orthopyroxene with zonal structure in the CAU230 specimen. (b) Results from the SEM-EDS elemental mapping for the orthopyroxene (a) with banded texture. Concentration of Mg is increasing from core to rim. (c) BSE image of the crystallite in the CAU229 specimen. (d–f) Results of elemental mapping for the crystallite in the CAU229 specimen. The composition of crystallite is rich in Ca, Fe and Mg with respect to the matrix glass.

nomenclature developed by Leake et al. (1997), all of the analyzed amphiboles are classified into the “tschermakite”.

5. Whole-rock chemistry

5-1 Sample preparation methodology

The whole-rock chemistry for the specimens containing

ol-bearing aggregate (i.e. CAU230 and 239 specimens), and the specimens free from ol-bearing aggregate (i.e. CAU29 specimens) was analyzed by means of WDXRF (Wavelength Dispersive X-ray Fluorescence Spectrometer). The model Rigaku ZSX Primus III+, located in the Center for Obsidian and Lithic Studies, Meiji University, was used for this analysis. Following the methodology was developed by Suda (2013), where the fusion bead with dilution rate (flux

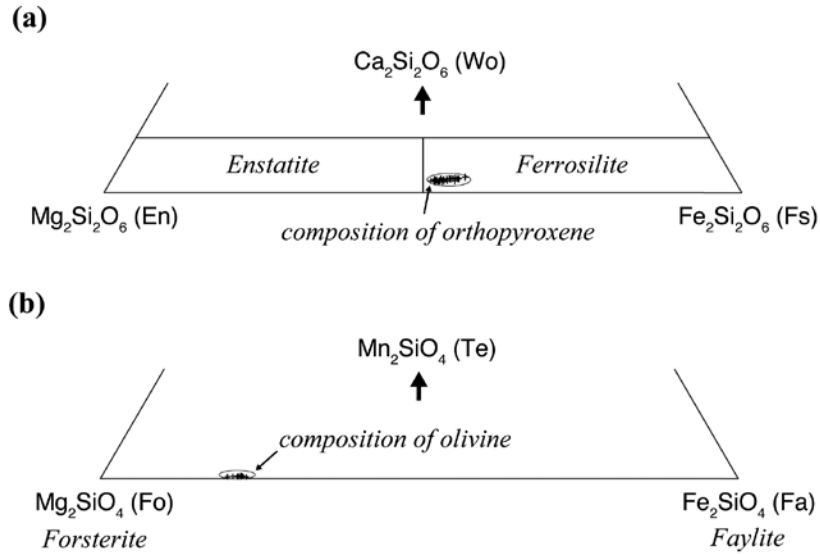


Figure 10 Ternary diagrams indicating the compositional variation of clinopyroxene (a) and olivine (b) in all specimens.

Table 3. Representative compositions of minerals by SEM-EDS analysis

mineral sample	olivine						orthopyroxene			ilmenite		
	CAU230		CAU239				CAU229	CAU230	CAU239	CAU229	CAU230	CAU239
	<i>ol-ag</i>	<i>ol-ag</i>	<i>ol-ag</i>	<i>ol-ag</i>	<i>ol-ag</i>	<i>ol-ag</i>	<i>opx-ag</i>	<i>opx-ag</i>	<i>opx-ag</i>	<i>opx-ag</i>	<i>opx-ag</i>	<i>pl-ag</i>
SiO ₂	38.93	38.93	38.39	38.36	38.32	38.32	50.74	50.32	50.78	0.24	0.17	0.16
TiO ₂	0.00	0.12	0.09	0.12	0.00	0.00	0.11	0.09	0.06	49.96	50.40	50.15
Al ₂ O ₃	0.00	0.00	0.00	0.05	0.00	0.00	0.72	0.96	0.67	0.18	0.21	0.25
FeO	19.93	20.56	21.71	21.37	22.60	22.15	32.07	32.79	32.43	47.34	46.70	47.43
MnO	0.28	0.32	0.50	0.33	0.24	0.30	1.06	1.04	0.93	0.76	1.02	0.75
MgO	40.68	39.85	39.17	39.71	38.64	39.05	14.24	13.60	14.05	1.27	1.40	1.10
CaO	0.16	0.21	0.12	0.07	0.17	0.19	1.02	1.13	1.08	0.09	0.04	0.10
Na ₂ O	0.00	0.00	0.00	0.00	0.03	0.00	0.04	0.04	0.00	0.15	0.06	0.05
K ₂ O	0.01	0.00	0.01	0.00	0.00	0.00	0.00	0.03	0.00	0.00	0.00	0.01
total	100.00	100.00	100.00	100.00	100.00	100.00	100.00	100.00	100.00	100.00	100.00	100.00
O =	4	4	4	4	4	4	6	6	6	3	3	3
Si	1.001	1.004	0.997	0.994	0.998	0.996	1.990	1.982	1.993	0.006	0.004	0.004
Ti	0.000	0.002	0.002	0.002	0.000	0.000	0.003	0.003	0.002	0.953	0.958	0.956
Al	0.000	0.000	0.000	0.002	0.000	0.000	0.033	0.045	0.031	0.005	0.006	0.007
Fe ²⁺	0.386	0.399	0.424	0.417	0.443	0.433	0.947	0.972	0.958	0.903	0.889	0.905
Mn	0.006	0.007	0.011	0.007	0.005	0.007	0.035	0.035	0.031	0.016	0.022	0.016
Mg	1.559	1.532	1.516	1.533	1.500	1.514	0.833	0.799	0.822	0.048	0.053	0.042
Ca	0.004	0.006	0.003	0.002	0.005	0.005	0.043	0.048	0.045	0.002	0.001	0.003
Na	0.000	0.000	0.000	0.000	0.002	0.000	0.003	0.003	0.000	0.007	0.003	0.002
K	0.000	0.000	0.000	0.000	0.000	0.000	0.000	0.002	0.000	0.000	0.000	0.000
Fo%	79.9	79.1	77.7	78.3	77.0	77.5						
Fa%	19.8	20.6	21.7	21.3	22.7	22.2						
Te%	0.3	0.4	0.6	0.4	0.3	0.3						
Wo%							2.4	2.6	2.5			
En%							45.7	43.9	45.0			
Fs%							52.0	53.5	52.5			

weight/sample weight ratio) of 4.000 was applied for the measurement of the whole-rock concentrations of the major oxides (SiO_2 , TiO_2 , Al_2O_3 , $\text{T-Fe}_2\text{O}_3$, MnO , MgO , CaO , Na_2O , K_2O and P_2O_5). The Merck Spectromelt A12 (di-lithium tetraborate 66% + lithium metaborate 34%) was used as the flux. The heating temperature was 120°C and the time for the absorbed water (H_2O^-) in samples to be removed was 12 hours. The pulverized samples were prepared using the methods detailed below.

Weathered and altered portions were removed with a rock-cutting saw (Maruto MC-420). The specimens were cut into a thin slab with ca. 2.0 mm in thickness using a precision rock-cutting saw (Struers Accutom-50). The cut surfaces were then

polished using a grinding machine (Maruto ML-110NT and 3M 400 mesh diamond disc). A total of 10–15g of the thin slabs were roughly pulverized using a vibratory micro mill (Fritsch P-0 with agate ball mill). The vibration time was ca. 3 minutes. Subsequently, the samples were further pulverized for ca. 3 minutes using the beat and mortar machine (Ishikawa AGB with agate bowl and agate beetle). The pulverized samples were kept in a glass bottle with 20 ml capacity. Additional description for the sample preparation can be found in Suda (2012, 2013, in press).

5-2 Results

The results of whole-rock analysis for the CAU229, 230

Table 4. Representative compositions of hornblende in CAU230 specimen, and results of P-T calculation

SiO_2	43.85	43.37	42.07	43.59	43.58	43.73
TiO_2	1.99	2.36	3.09	2.89	1.75	2.75
Al_2O_3	11.93	12.04	13.23	12.16	12.83	11.74
FeO^*	15.10	15.85	15.36	15.30	15.67	15.26
MnO	0.36	0.23	0.27	0.08	0.03	0.23
MgO	13.31	12.43	11.73	12.25	12.56	12.85
CaO	11.07	11.38	11.69	11.14	11.31	11.05
Na_2O	1.80	1.71	1.81	1.84	1.67	1.81
K_2O	0.58	0.64	0.74	0.74	0.59	0.57
Total	100.00	100.00	100.00	100.00	100.00	100.00
T-site						
Si	6.18	6.18	6.04	6.21	6.17	6.20
Al^{IV}	1.82	1.82	1.96	1.79	1.83	1.80
M1, M2, M3 sites						
Al^{VI}	0.17	0.19	0.28	0.25	0.31	0.16
Ti	0.21	0.25	0.33	0.31	0.19	0.29
Fe^{3+}	1.29	1.07	0.78	0.87	1.16	1.11
Mn	0.04	0.03	0.03	0.01	0.00	0.03
Mg	2.80	2.64	2.51	2.60	2.65	2.71
Fe^{2+}	0.50	0.82	1.07	0.95	0.69	0.70
M4 site						
Ca	1.67	1.74	1.80	1.70	1.71	1.68
Na	0.33	0.26	0.20	0.30	0.29	0.32
A site						
Na	0.17	0.21	0.30	0.21	0.17	0.17
K	0.10	0.12	0.14	0.13	0.11	0.10
$T_{\text{HB}} (^\circ\text{C})$	1216	1256	1358	1226	1185	1229
P_s (kbar)	6.4	6.6	7.6	6.7	7.2	6.3
P_j (kbar)	4.9	5.1	6.0	5.2	5.6	4.8
P_h (kbar)	6.4	6.6	7.9	6.8	7.3	6.3
P_{hz} (kbar)	6.1	6.2	7.3	6.4	6.8	5.9

Abbreviations: T_{HB} , Holland and Blundy (1994); P_s , Schmidt (1992); P_{AS} , Anderson and Smith (1995)

and 239 specimens are shown in Table 5. The methodology used to determine whole-rock composition with the WDXRF method has recently been described by Suda (2013). This analysis was performed to make the two fusion beads per one specimen. The measurements were repeated three times for each bead average value of all the results is used as the final result. Precision and errors in the final values were also estimated in order to calculate the standard deviation (2σ) for all results.

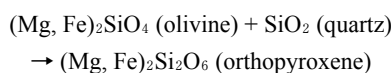
The compositional variation diagrams with respect to the concentration of SiO_2 can be found in Figure 11. The $\text{Na}_2\text{O}+\text{K}_2\text{O}$ versus SiO_2 diagram (Figure 11a) indicates that the samples have rhyolitic composition, and can be classified under the subalkaline rock series (Miyashiro 1978; Le Maitre 2002). The SiO_2 wt.% contents are quite uniform, ranging from 70.71 to 71.15. On the K_2O versus SiO_2 diagram (Figure 11b), these specimens are classified into the high-K calc-alkaline rock series (Le Maitre 2002). The K_2O wt.% contents range from 3.70 to 3.76.

Whole-rock compositions of the mafic xenolith (ol-bearing aggregate) were estimated after the modal compositions of the olivine, plagioclase and amphibole, and the chemistry of these minerals (Appendix 2). The calculated compositions of the mafic xenolith, and the composition of Ukraine Transcarpathian obsidian (i.e. analyzed specimens) are plotted in the $\text{MgO}+\text{T-Fe}_2\text{O}_3$ versus SiO_2 diagram (Figure 11c). The result indicates that the whole-rock composition of the $\text{MgO}+\text{T-Fe}_2\text{O}_3$ is slightly influenced by the modal composition of the mafic xenolith in the specimens. Indeed, the specimen with the most abundant quantity of mafic xenolith (CAU230 specimens) are relatively enriched in the $\text{MgO}+\text{T-Fe}_2\text{O}_3$ content and plotted on the mixing line with the mafic xenolith (Figure 11c).

6. Discussion

6-1 Origin of ol-bearing aggregate (mafic xenolith)

The compositional relation between olivine and orthopyroxene is expressed by the following chemical equilibria (Enami 2013: p.35):



This relation indicates that the olivine cannot generally coexist with the SiO_2 phase. Therefore, the olivine will predominantly exist in basic and ultrabasic rocks (i.e. SiO_2 poor rocks). On the other hand, the Fe-rich orthopyroxene becomes quite unstable under pressure and temperature

conditions that fall below the solidus line of general felsic magma. Such conditions are not favorable for the occurrence of orthopyroxene, but they provide a suitable environment for the Fe-rich olivine with quartz. Therefore, the occurrence of Mg-rich olivine in obsidian of rhyolitic composition is quite unusual in the context of its textural setting.

Microscopic analysis indicates that the olivine is found to occur predominantly in association with the Na-rich plagioclase and amphibole. Such occurrence and the composition of the olivine suggest that the ol-bearing aggregate is fundamentally an exotic material, or that the “xenolith” derived from the gabbroic rocks in the lowermost

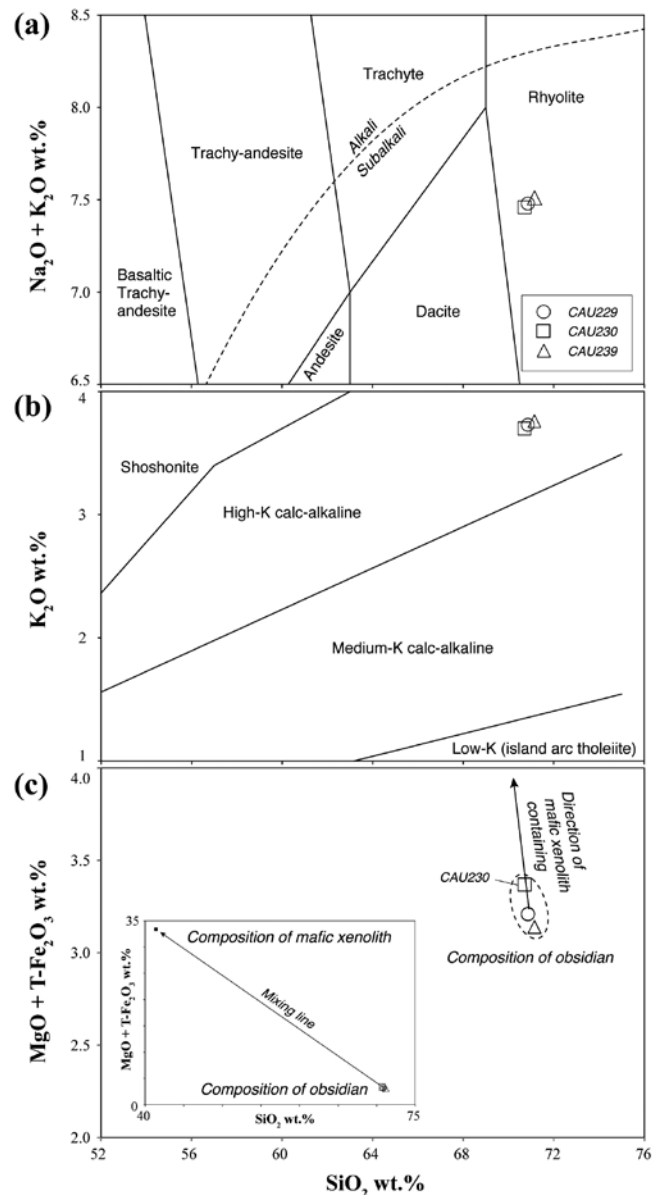


Figure 11 Variations of $\text{Na}_2\text{O}+\text{K}_2\text{O}$ (a), K_2O (b), and $\text{MgO}+\text{T-Fe}_2\text{O}_3$ (c) contents with respect to the SiO_2 content. Discrimination fields and nomenclatures in (a) and (b) are after Miyashiro (1978) and Le Maitre (2002).

crust beneath the Carpathian arc.

On the basis of the elemental composition of the amphibole and the coexisting plagioclase, the pressure and temperature conditions of the gabbroic xenolith were estimated using geothermobarometry (Hammarstrom and Zen 1986; Hollister et al. 1987; Johnson and Rutherford 1989; Schmidt 1992; Holland and Blundy 1994; Anderson and Smith 1995). The results of these calculations are shown in Table 3. We followed the methodology of Suda (2004: p.356) for the calculation of the temperature conditions (Holland and Blundy 1994), which were calculated based on the An90% in plagioclase.

The result indicates that the estimated temperature is 1185–1358°C, while the pressure is 4.5–7.9kbar. These conditions suggest that gabbroic xenolith found in the specimens is solidified at the deeper crustal level of 20–30km in depth. This depth corresponds to the lower crust or lowermost crust of an island arc (e.g. Takahashi 2007). The genesis of this gabbroic or mafic xenolith does not correlate with the genesis of the rhyolitic magma that became the source of the obsidian in the Carpathian volcanic arc region.

6-2 Origin of Ca-rich plagioclase

Microscopic observation has shown that the Ca-rich plagioclase (i.e. An content >89%) is characterized by compositionally homogenous crystals lacking the zonal structure (Figure 8; Table 2). Furthermore, these plagioclase grains are found either as isolated phenocrysts, or in the ol-bearing aggregate (mafic xenolith). Elemental compositions of this type of Ca-rich plagioclase do not overlap with those of the plagioclase with zonal structure.

These results suggest that the genesis of all Ca-rich plagioclase occurring in the specimens is homogenous, even though their occurrences vary. Ca-rich plagioclase occurring as isolated phenocrysts would have originated from the ol-bearing aggregate or the mafic xenolith, which is also a relic of the lower crustal components underneath the Carpathian volcanic arc.

7. Conclusions

1. The obsidian in the Tolstoi-Tupoi volcanic mountain, at the northwestern part of Khust City, is characterized by the occurrence of mafic or gabbroic xenolith comprising of Mg-rich olivine + Ca-rich plagioclase + amphibole (tschermakite).
2. The temperature and pressure conditions of the mafic xenolith are estimated to be 1185–1358°C and 4.5–7.9kbar, respectively. The conditions are the equivalent of the conditions of the crust of 20–30 km in depth, which corresponds to the lower crustal level of an island arc.
3. The mafic xenoliths found in the obsidian originated from the lower crustal components or gabbroic rock underneath the Carpathian volcanic arc. This mafic xenolith would become a key in reconstructing the tectonic history of the Alpine orogeny in the Transcarpathian region, and would also help to reveal the petrogenesis of the obsidian or rhyolitic magma in this area.

Acknowledgements

This study was supported by Grants-in-Aid for International Research Promotion from Meiji University in 2013, and by a grant from the Strategic Research Foundation Grant-aided Project for Private Universities from Ministry of Education, Culture, Sport, Science, and Technology of Japan (MEXT), 2011–2016 (S1101020), and partly supported by grant 53.5/005-2013 by the State Fund for Fundamental Researches, Ukraine.

The manuscript was improved by the constructive reviews and comments by Prof. Dr. M. Satish Kumar (Niigata University, Japan). We extend our sincere thanks to the following colleagues: Dr. T. Hokada (National Institute of Polar Research, Japan) for conducting the EPMA analysis; Ms. L. Dogiama (McMaster University, Canada) for improving an earlier version of the manuscript; Mr. Pavel Levchuk (Institute of Archaeology, Ukraine) for supporting the fieldwork in the Transcarpathian area; and to Prof. Dr. A. Ono (Meiji University, Japan) for coordinating this research project on Carpathian obsidian. Special thanks also go to Mr. J. Hashizume and Ms. M. Tsuchiya (Meiji University, Japan) for editing this article.

References

- Anderson, J. L. and Smith, D. R. 1995 The effects of temperature and fO_2 on the Al-in-hornblende barometer. *American Mineralogist* 80: 549–559.
- Enami, M. 2013 *Introduction to Modern Earth Science Series vol. 16 Petrology*. 254p., Tokyo, Kyoritsu Shuppan (in Japanese).
- Foldvary, G. Z. 1988 *Geology of the Carpathian region*, 571p., Teaneck (USA), World Scientific.
- Hammarstrom, J. M. and Zen, E. 1986 Aluminium in hornblende: An empirical igneous geobarometer. *American Mineralogist* 71: 1297–1313.
- Gladilin, V. N. and Sitlivyj, V. I. 1990 *Achel Tzentralnoy Evropu [The Acheulian of Central Europe]*, 267p., Kiev, Naukova dumka.
- Holland, T. and Blundy J. 1994 Non-ideal interactions in calcic amphiboles and their bearing on amphibole-plagioclase thermometry. *Contributions to Mineralogy and Petrology* 116: 433–447.
- Hollister, L. S., Grisson, G. C., Peters, E. K., Stowell, H. H. and Sisson, V. B. 1987 Confirmation of the empirical correlation of Al in hornblende with pressure of solidification of calc-alkaline plutons. *American Mineralogist* 72: 231–239.
- Jackson, J. A. (editor) 1997 *Glossary of Geology* Fourth edition,

- 769p., Alexandria (USA), American Geological Institute.
- Johnson, M. C. and Rutherford, M. J. 1989 Experimental calibration of aluminum-in-hornblende geobarometer with application to Long Valley caldera (California) volcanic rocks. *Geology* 17: 837–841.
- Konecny, V., Kovac, M., Lexa, J. and Sefara, J. 2002 Neogen evolution of the Carpatho-Pannonian region: an interplay of subduction and back-arc diapiric uprise in the mantle. *EGU Stephan Mueller Special Publication Series* 1: 105–123.
- Le Maitre, R. W. 2002 Igneous rocks – a classification and glossary of terms. Recommendations of the IUGS subcommission on Systematics of Igneous rocks 2nd edition, 256p., Cambridge: Cambridge University Press.
- Leake, B. E., Woolley, A. R., Arps, C. E. S., Birch, W. D., Gilbert, M. C., Grice, J. D., Hawthorne, F. C., Kato, A., Kisch, H. J., Krivovichev, V. G., Linthout, K., Laird, J., Mandarino, J., Maresch, Nickel, E. H., Rock, N. M. S., Schumacher, J. C., Smith, D.C., Stephenson, N. C. N., Ungaretti, L., Whittaker, E. J. W. and Youzhi G. 1997 Nomenclature of amphiboles: report of the subcommittee on the international mineralogical association, commission on new minerals and mineral names. *Mineralogical Magazine* 61: 295–321.
- Lexa, J., Seghedi, L., Nemeth, K., Szakacs, A., Konecny, V., Pecskey, Z., Fulop, A. and Kovacs, M. 2010 Neogene-Quaternary volcanic forms in the Carpathian-Pannonian Region: a review. *Central European Journal of Geosciences* 2(3): 207–270.
- Mason, P. D., Seghedi, I., Szakacs, A. and Downes, H. 1998 Magmatic constraints on geodynamic models of subduction in the East Carpathians, Romania. *Tectonophysics* 297: 157–176.
- Miyashiro, A. 1978 Nature of alkali volcanic rock series. *Contributions to Mineralogy and Petrology* 66: 91–104.
- Oszczypko, N. 2004 The structural position and tectonosedimentary evolution of the Polish Outer Carpathians. *Przegląd Geologiczny* 52: 780–791.
- Pecskey, Z., Lexa, J., Szakacs, A., Seghedi, I., Balogh, K., Konecny, V., Zelenka, T., Kovacs, M., Poka, T. and Fulop, A. 2006 Geochronology of Neogene magmatism in the Carpathian arc and intra-Carpathian area. *Geologica Carpathia* 57(6): 511–530.
- Pecskey, Z., Seghedi, I., Downes, H., Prychodko, M., Mackiv, B. 2000 K/Ar dating of neogene calc-alkaline volcanic rocks from Transcarpathian Ukraine. *Geologica Carpathica* 51: 83–89.
- Pecskey, Z., Seghedi, I., Kovacs, M., Szakacs, A. and Fulop, A. 2009 Geochronology of the Neogene calc-alkaline intrusive magmatism in the “Subvolcanic Zone” of the Eastern Carpathians (Romania). *Geologica Carpathia* 60(2): 181–190.
- Rasser M. W. and Harzhauser M. 2008 *In Geology of Central Europe: Paleogene and Neogene of Central Europe vol. 2*, pp.1030–1139, Mesozoic and Cenozoic, London, Geol. Soc. London, Publ. House.
- Rosania, C. N., Boulanger, M. T., Biro, K. T., Ryzhov, S., Trnka, G. and Glascock, M. D. 2008 Revisiting Carpathian obsidian. *Antiquity* 82: 318.
- Rosenbaum, G. and Lister, G. S. 2002 Reconstruction of the evolution of the Alpine-Himalayan Orogen – an introduction. *Journal of the Virtual Explorer* 8: 1–2.
- Ryzhov, S., Matviishina, J. N., Pudovkina, A. S. and Levchuk, P. A. 2009 The study stratigraphy and planigraphy of the Malyj Rakovets IV site in Transcarpathia. *Vita Antiqua* 7–8: 60–71 (in Russian with English abstract).
- Ryzhov, S., Stepanchuk, V. and Sapozhnikov, I. 2005 Raw materials provenance in Palaeolithic of Ukraine: approaches and first results. *Archaeometrial Miehelu* 4: 17–25.
- Ryzhov, S. 2012 Obsidian Outcrops in Transcarpathia and their Use during the Paleolithic Time. *Natural Resource Environment and Humans* 3: 125–126.
- Schmid, S. M., Fugenschuh, B., Kissling, E., and Schuster, R. 2004 Tectonic map and overall architecture of the Alpine orogen. *Eclogae Geologicae Helveticae* 97: 93–117.
- Schmid, S. M., Bernoulli, D., Fugenschuh, B., Matenco, L., Schefer, S., Schuster, R., Tischler, M. and Ustaszewski, K. 2008 The Alpine-Carpathian-Dinaridic orogenic system: correlation and evolution of tectonic units. *Swiss Journal of Geosciences* 101(1): 139–183.
- Schmidt, M. W. 1992 Amphibole composition in tonalite as a function of pressure: an experimental calibration of the Al-in-hornblende barometer. *Contributions to Mineralogy and Petrology* 110: 304–310.
- Seghedi, I., Downes, H., Szakacs, A., Mason, P. D., Thirlwall, M. F., Rosu, E., Pecskey, Z., Marton, E. and Panaiotu, C. 2004 Neogene-Quaternary magmatism and geodynamics in the Carpathian-Pannonian region: a synthesis. *Lithos* 72: 117–146.
- Shcherbakov, V. D., Plechov, P. Y., Izbekov, P. E., and Shipman, J. S. 2011 Plagioclase zoning as an indicator of magma processes at Bezymianny Volcano, Kamchatka. *Contributions to Mineralogy and Petrology* 162: 83–99.
- Siliviy, V. and Ryzhov, S. 1992 The late middle Palaeolithic complex of Malyj Rakovets IV in Transcarpathia (Preliminary results). *Archäologisches Korrespondenzblatt* 22: 301–314.
- Stepanchuk, V., Ryzhov, S., Rekovets, L., Matviishina, Z. 2010 The Lower Palaeolithic of Ukraine: Current Evidence. *Quaternary International* 223–224: 131–142.
- Streckeisen, A. L. 1976 To each plutonic rock its proper name. *Earth-Science Reviews* 12: 1–33.
- Suda, Y. 2004 Crustal anatexis and evolution of granitoid magma in Permian intra-oceanic island arc, the Asago body of the Yakuno ophiolite, Southwest Japan. *Journal of Mineralogical and Petrological Sciences* 99: 339–356.
- Suda, Y. 2012 Chemical analysis of obsidian by Wave Length-dispersive X-ray Fluorescence Spectrometry: application to nondestructive analysis of archeological obsidian artifacts. *Natural Resource Environment and Humans* 2: 1–14.
- Suda, Y. 2013 Quantitative analytical methodology for major elements in silicate rocks by wavelength dispersive X-ray

- fluorescence spectrometry. *Natural Resource Environment and Humans* 3: 31–45 (in Japanese with English abstract).
- Suda, Y. Application of internal standard method to non-destructive analysis of obsidian artifacts by Wavelength dispersive X-ray fluorescence Spectrometry. In *Methodological issues for characterisation and provenance studies of obsidian in Northeast Asia*, edited by A. Ono, M. D. Glascock, Y. V. Kuzmin and Y. Suda, Oxford (UK), Archaeopress (in press).
- Takashi, N., Kodaira, S., Klemperer, L., Tatsumi, Y., Kaneda, Y. and Suyehiro, K. 2007 Crustal structure and evolution of the Mariana intra-oceanic island arc. *Geology* 35(3): 203–206.
- Yamada, M. 2012 Notes on the studies of lithic raw material sources: a case of European Upper Paleolithic. *Natural Resource Environment and Humans* 2: 37–48 (in Japanese with English abstract).
- Yamada, M. 2013 Obsidian studies in the Mediterranean region: an overview of research. *Natural Resource Environment and Humans* 3: 47–64 (in Japanese with English abstract).

(Received 3 December 2013 / Accepted 15 January 2014)

Appendix 1. Comparison between SEM-EDS and EPMA results

Sample Mineral Method	JOR-1 (Shirataki, Rubeshibe)				JOSH-1 (Shirataki, Hachigo-sawa)			
	plagioclase		ilmenite		olivine		glass	
	SEM-EDS	EPMA	SEM-EDS	EPMA	SEM-EDS	EPMA	SEM-EDS	EPMA
SiO ₂	58.80	57.42	0.56	0.15	30.53	29.96	80.39	79.32
TiO ₂		0.03	11.63	10.45	0.10	0.14	0.08	0.06
Al ₂ O ₃	26.24	26.33	2.44	2.27	0.28	0.13	13.32	13.03
FeO	0.15	0.18	84.35	80.76	64.18	65.35	0.32	0.37
MnO		0.04	0.19	0.61	3.43	3.30	0.16	0.07
MgO	0.05	0.00	0.41	0.30	1.33	1.38	0.02	0.01
CaO	7.96	8.40	0.11	0.16	0.00	0.07	0.53	0.52
Na ₂ O	6.40	6.54	0.20	0.04	0.07	0.03	0.47	1.52
K ₂ O	0.41	0.38	0.10	0.05	0.08	0.07	4.71	4.20
total	100.01	99.32	99.99	94.78	100.00	100.43	100.00	99.10
O =	8	8	3	3	4	4		
Si	2.625	2.592	0.018	0.005	1.014	0.999		
Ti	0.000	0.001	0.277	0.266	0.002	0.004		
Al	1.381	1.401	0.091	0.090	0.011	0.005		
Fe ²⁺	0.005	0.006	2.013	2.054	1.605	1.639		
Mn	0.000	0.002	0.005	0.018	0.097	0.093		
Mg	0.003	0.000	0.019	0.015	0.066	0.069		
Ca	0.381	0.406	0.004	0.006	0.000	0.003		
Na	0.554	0.572	0.012	0.003	0.005	0.002		
K	0.023	0.022	0.004	0.002	0.003	0.003		

Appendix 2. Calculation for the whole-rock compositions (in wt.%) of mafic xenolith (ol-bearing aggregate)

	fraction	SiO ₂	TiO ₂	Al ₂ O ₃	*T-Fe ₂ O ₃	MnO	MgO	CaO	Na ₂ O	K ₂ O	total
Plagioclase	0.30	45.35	0.03	34.97	0.52	0.02	0.07	18.12	0.91	0.01	100.00
Hornblende	0.30	42.37	2.44	12.19	16.86	0.28	12.28	11.19	1.74	0.64	100.00
Olivine	0.40	37.67	0.06	0.00	22.90	0.28	38.89	0.19	0.00	0.01	100.00
Calculated composition		41.38	0.76	14.15	14.37	0.20	19.26	8.87	0.80	0.20	100.00

*: Fe as total Fe₂O₃

ウクライナ，トランスカルパチア地方における 黒曜石の記載岩石学的特徴

隅田祥光^{1*}・山田昌功²

S. リゾフ³・V. ステパンチューク⁴

要 旨

筆者らは、ウクライナ、トランスカルパチア地方における黒曜石の地質調査と岩石学にかんする研究を実施した。この地域の黒曜石中にはマグネシウムに富むかんらん石、カルシウムに富む斜長石、チェルマーク角閃石により構成される苦鉄質捕獲岩がしばしば含まれる。鉱物組合せと元素組成に基づくと苦鉄質捕獲岩は斑れい岩類に相当し、斜長石-角閃石地質温度圧力計から4.5-7.9kbar, 1185-1358°Cの形成条件が見積もられた。この苦鉄質捕獲岩は、カルパチア火山弧の下部地殻を構成していた斑れい岩類に由来するものであろうと想定され、新第三紀におけるカルパチア地方のテクトニクスを明らかにする上で重要な情報源になるであろう。

キーワード：黒曜石，トランスカルパチア，ウクライナ，地質学，岩石記載，地球化学

(2013年12月3日受付／2014年1月15日受理)

-
- 1 明治大学黒曜石研究センター
〒386-0601 長野県小県郡長和町大門 3670-8
 - 2 明治大学黒曜石研究センター猿楽町分室
〒101-0064 東京都千代田区神田駿河台 1-1
 - 3 ウクライナ国立タラス・シェフチェンコ・キエフ大学
Olodymirska St. 64. Kyiv 01601, Ukraine
 - 4 国立ウクライナ科学アカデミー考古学研究所
Geroiv Stalingrada ave., 04210, Kyiv-210, Ukraine
- * 責任著者：隅田祥光 (geosuda@gmail.com)